Carbohydrate Research 344 (2009) 374–383

Contents lists available at ScienceDirect

Carbohydrate Research

journal homepage: www.elsevier.com/locate/carres

DFT conformation and energies of amylose fragments at atomic resolution. Part 2: 'band-flip' and 'kink' forms of α-maltotetraose

Udo Schnupf, J. L. Willett, Frank A. Momany *

Plant Polymer Research, USDA,† ARS, National Center for Agricultural Utilization Research, 1815 N. University St., Peoria, IL 61604, USA

ARTICLE INFO

Article history:
Received 8 September 2008
Received in revised form 6 November 2008
Accepted 19 November 2008
Available online 9 December 2008

Keywords:
DFT
B3LYP/6-311++G**
DP-4
α-Maltotetraose
Band-flip
Kink

ABSTRACT

In Part 2 of this series of DFT optimization studies of α-maltotetraose, we present results at the B3LYP/6-311++G** level of theory for conformations denoted 'band-flips' and 'kinks'. Recent experimental X-ray studies have found examples of amylose fragments with conformations distorted from the usual syn forms, and it was of interest to examine these novel structural motifs by the same high-level DFT methods used in Part 1. As in Part 1, we have examined numerous hydroxymethyl rotamers (gg, gt, and tg) at different locations in the residue sequence, and include the two hydroxyl rotamers, the clockwise 'c' and counterclockwise 'r' forms. A total of fifty conformations were calculated and energy differences were found to attempt to identify those sources of electronic energy that dictate stressed amylose conformations. Most stressed conformations were found to have relative energies considerably greater (i.e., ~4 to 12 kcal/mol) than the lowest energy syn forms. Relative energy differences between 'c' and 'r' forms are somewhat mixed with some stressed conformations being 'c' favored and some 'r' favored, with the lowest energy 'kink' form being an all-gg-r conformation with the 'kink' in the *bc* glycosidic dihedral angles. Comparison of our calculated structures with experimental results shows very close correspondence in dihedral angles.

Published by Elsevier Ltd.

1. Introduction

In the previous paper, Part 1,[1] the syn form of α-maltotetraose was studied by density functional geometry optimization methods at the B3LYP/6-311++G** level of theory. Recently,[2–5] strain-induced 'band-flips' in large cyclic α-(1→4)-linked structures have been found using X-ray diffraction methods. An anti-glycosidic bond conformation was found in these cyclic structures, with the ψ_H position (C1–O1–C4′–H4′) rotated to ~180°. These novel structural motifs are denoted as 'band-flip' conformations, and are of interest as they add to our understanding of possible conformational features for carbohydrates. Further, structural motifs in which 'kink' conformations[4,5] were found, that is, conformations with glycosidic bond dihedral angles (ϕ_H/ψ_H) are twisted from the syn form by −40° to −50°, have also been observed experimentally.[4,5] Here, we computationally examine these two types of stress-induced forms of amylose using our previously described density functional theory (DFT). In particular, we are interested in finding the energetically preferred hydroxyl and hydroxymethyl rotamers in order to compare structural information with that of the low-energy syn forms described in Part 1.[1]

As noted previously, α-maltotetraose is a four-glucose residue fragment of amylose and is found to have nutritional and dietetic significance[6–9] as well as other uses.

The density functional methods used here were described in Part 1, and will not be repeated in detail here. Fifty different conformations are presented here with 'band-flip' or 'kink' conformations at different positions in the residue sequence of syn conformations. This work is a continuation of an extensive series of conformational studies on carbohydrates at a high level of theory.[10–24] Properties of interest include internal coordinates, electronic energy, and conformational characteristics of these important carbohydrates. Only $^4C_1$ glucose ring structures are included in this work, maintaining the α-(1→4) linkage throughout and varying the hydroxymethyl and hydroxyl groups as described previously.[1] Further, we are pointing to the fact that starting conformations are particularly important because of the small energetically allowed conformational regions for these higher energy forms. In these stressed high-energy cases, small variations in dihedral angles from the minimum energy position will cause considerable difficulty in the optimization cycles. A number of different gg and gt forms are optimized, but only a few selected conformations with tg hydroxymethyl groups are examined, in particular, those combinations that may have favorable energy, as determined from previous studies.[21–24] Optimizations are

* Corresponding author. Tel./fax: +1 309 681 6362.
E-mail address: frank.momany@ars.usda.gov (F.A. Momany).

† Names are necessary to report factually on available data; however, the USDA neither guarantees nor warrants the standard of the product, and the use of the name by USDA implies no approval of the product to the exclusion of others that may also be suitable.

0008-6215/$ - see front matter Published by Elsevier Ltd.
doi:10.1016/j.carres.2008.11.016

carried out in vacuo and solvated (solvation in bulk water is simulated via an implicit solvation model) states because carbohydrates are found in nature with different hydration levels, whereas low hydration levels are best described by in vacuo calculations.

2. Computational methodology

The starting conformations are generated as described previously,[1] and the rationale for choosing combinations of hydroxymethyl and hydroxyl groups is presented in Part 1 of this series. DFT calculations are carried out using B3LYP as the density functional, and moving from the smaller basis set (B3LYP/6-31+G*) to the larger basis set (B3LYP/6-311++G**) during optimization. Parallel Quantum Solutions[25] software and hardware (QS4-2000S, QS8-2600S, and QS16-2600S) were utilized. Results are reported only for the larger basis set, since the results for the two different sets are very close in this series of molecules. The standard convergence criteria are the same as previously reported.[1] During modeling,[26] only homodromic hydroxyl group rotamers were studied; thus the conformations are either all-c (clockwise) or all-r (counterclockwise) forms. Hydroxymethyl groups are defined as gg, gt, and tg.[1] Figures were prepared as in Part 1.[27]

2.1. Selecting starting conformations

As before,[1] all rings are taken to be $^4C_1$, and in-house empirical potentials (AMB06C) are used to find and briefly optimize starting conformations. The source of starting structures was data on 'band-flips' and 'kink' structures in several recent publications on maltose.[21–23] In the DFT iso-energetic contour maps of maltose, obtained from energy versus glycosidic dihedral angles, minimum energy ϕ_H/ψ_H space was much smaller around the 'band-flip' conformations than the regions of low energy found for the syn forms. Further, it was observed that at the particular minimum energy position, one could use specific combinations of hydroxymethyl groups to stabilize 'band-flip' conformers. Further, from experimental[2,3] X-ray results of large cyclic amylose structures, for example, CA26, it was possible to compare our calculated 'band-flip' conformations with experimental 'band-flip' structures, and that led to other low-energy starting conformations.

3. Results

3.1. 'Band-flip' conformations

The lowest energy 'band-flip' conformation without including tg rotamers (Fig. 1) has a relative energy, (ΔE), ~5.3 kcal/mol higher than the lowest energy syn conformation found previously[1] (see Table 1). All 'band-flip' conformers are in the *bc* glycosidic bond region, that is, the middle glycosidic bond in DP-4. Relative energies of 5.8 kcal/mol occur in the all-gg-c form, 5.3 kcal/mol in gg–gt–gg–gg-c (Fig. 1), 5.9 kcal/mol in gg–gg–gt–gg-c, 5.3 kcal/mol in gg–gt–gt–gg-c, and 5.2 kcal/mol in gg–gt–tg–gg-c, the latter having a tg group immediately following the 'band-flip' glycosidic bond ($\phi_H \sim -35°$; $\psi_H \sim -176°$). Two conformers similar to the last form mentioned above let us compare the effect of the hydroxymethyl rotamer on position. The one having tg in the *a* position does not reduce the ΔE, but in fact raises it to 6.5 kcal/mol, while putting a gt in the *a* position also raises the relative energy to 6.5 kcal/mol. In all cases studied, the 'c' form is of lower energy than the 'r' form, for 'band-flip' structures. Since the difference between the 'c' and 'r' forms is rather large ($\Delta\Delta E \sim 1.6$ kcal/mol for the all-gg case, ~2.5 kcal/mol for the gg–gt–gg–gg-c/r case, and ~4.4 kcal/mol for the gg–gt–gt–gg-c/r case), and similarly for others, it would appear that there is an energy effect present in the 'band-flip' case that is not present in the syn conformers. This magnitude of difference is not found in the normal syn type conformations, with the exception of the application of the solvation methods (i.e., COSMO).[28] It is not clear that even when COSMO is applied, this large energy difference will be overcome to allow the 'r' forms to be of lower energy than the 'c' forms.

'Band-flip' dihedral angles (ϕ_H/ψ_H) were found to have distinct differences between the 'c' and 'r' forms, ranging from $\phi_H \sim -23°$ to $-34°$ and $\psi_H \sim -152°$ to $-172°$ in the 'c' form, to $\phi_H \sim -32°$ to $-54°$ and $\psi_H \sim -164°$ to $-179°$ in the 'r' form, these values are taken from the lower energy 'band-flip' forms and the hydroxymethyl group conformation on the *c* residue. The syn ϕ_H/ψ_H values between the *ab* and *cd* residues do not vary significantly from those found in Part 1 of this series.

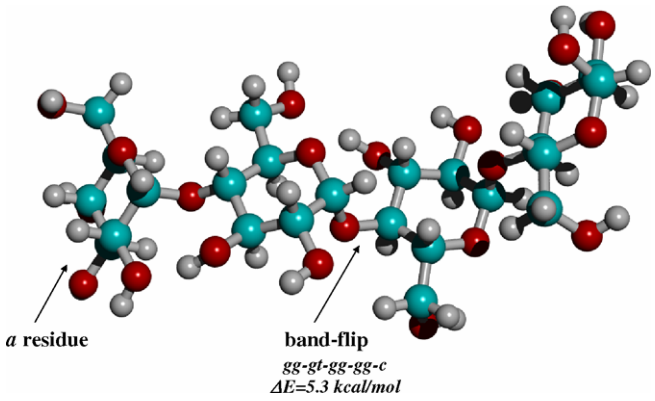

Figure 1. B3LYP/6-311++G** geometry optimized 'c' type DP-4 amylose fragment showing a band-flip in the center of the molecule.

3.2. 'Kink' conformations

The lowest energy conformation (Fig. 2) found in this work is the all-gg-r 'kink' form (see Table 2) with the distorted dihedrals between the *b* and *c* residues. The relative energy of ~3.7 kcal/mol is easily the lowest energy stressed form of the 'kink' structures of Table 2. The 'kink' conformation was shown to be a local energy minimum in ϕ_H/ψ_H maps of maltose[23] in the 'r' form. However, in contrast to maltose, in the DP-4 series, both 'c' and 'r' forms have energy minimum with 'kinks' between the middle residues. On the other hand, no stable 'kink' forms were found for the 'c' conformers when the 'kink' is placed between the *ab* positions. 'Kink' dihedral angles are generally in the $\phi_H \sim -45°$ to $-56°$ range and $\psi_H \sim -39°$ to $-45°$ range for both 'c' and 'r' forms, at least for the lower energy forms. Conformations with much higher relative energies were found, but are of little interest since they would not be part of a population of allowed structures. When the 'kink' is placed between the *ab* residues, the relative energies are quite modest, ranging from a value of ~4 to ~8 kcal/mol. The ϕ_H/ψ_H values for the 'r' 'kinks' are around $-43°/-40°$, respectively. It is interesting that when tg is placed in the *a* or end residue the relative energy is not improved, in discordance with the advantage tg has at this position in the all syn forms.

3.3. 'Band-flip/kink' combinations

Mixing both stressed conformations in the same molecule (see Fig. 3 and Table 3) was of interest since it was not clear if a 'band-flip' required a 'kink' in the post- or pre-residue sequence. No low relative energy form was found when the 'kink' was placed before or after the 'band-flip', with the all-gg-r having the lowest relative energy of ~8.9 kcal/mol. with the 'kink' following the 'band-flip'. The values of the glycosidic dihedral angles are nearly unperturbed

Table 1
B3LYP/6-311++G** relative energies, conformations (ϕ_H/ψ_H dihedral angles in °), and dipole moments of 'band-flip' type DP-4 amylose fragments

Conformer	Dihedral angles[a]						ΔE[b] (kcal/mol)	Dipole (Debye)
	$\phi_{H1}{}^{ab}$	$\psi_{H4}{}^{ab}$	$\phi_{H1}{}^{bc}$	$\psi_{H4}{}^{bc}$	$\phi_{H1}{}^{cd}$	$\psi_{H4}{}^{cd}$		
All gg, gt, and tg								
gg–gg–gg–gg-c	−7.3	−17.4	−23.0	−156.8	−9.2	−17.9	5.8	5.2
gg–gg–gg–gg-c′[c]	−7.3	−18.9	−23.4	−156.3	−7.7	−15.3	7.4	4.6
gg–gg–gg–gg-r	1.0	17.0	−40.5	−179.3	5.2	15.1	7.8	13.8
gt–gt–gt–gt-c	−7.8	−26.1	−29.3	−172.8	−8.8	−25.8	7.6	9.4
gt–gt–gt–gt-r	−10.1	5.6	−54.6	159.4	30.3	13.0	9.4	3.7
gt–gt–gt–gt-r′[d]	3.8	18.1	−32.8	−160.2	2.7	10.4	14.5	12.3
tg–tg–tg–tg-c	−6.8	−2.3	−30.8	−149.0	−5.4	3.8	10.8	12.5
tg–tg–tg–tg-c'	−7.0	−2.8	−30.6	−149.5	−5.1	−2.4	12.0	10.7
tg–tg–tg–tg-r	0.7	16.1	−23.7	−164.5	0.4	13.6	11.5	9.2
Mixed gg and gt								
gg–gt–gg–gg-c	−8.2	−21.8	−26.2	−167.0	−7.9	−17.5	5.3	8.5
gg–gt–gg–gg-r	−4.5	13.8	−32.0	−162.8	5.7	12.6	8.8	14.4
gg–gg–gt–gg-c	−7.1	15.5	−23.6	−156.3	−11.1	−13.6	5.9	6.9
gg–gg–gt–gg-r	0.9	17.1	−41.4	−178.4	0.2	10.4	8.0	11.9
gg–gt–gt–gg-c	−8.1	−24.3	−29.0	−172.6	−9.6	−13.9	5.3	8.1
gg–gt–gt–gg-r	−3.9	14.9	−41.7	−176.0	−15.3	−17.6	9.7	11.3
gt–gg–gg–gt-c	−10.0	−17.9	−22.6	−156.6	−10.5	−22.2	6.9	6.5
gt–gg–gg–gt-r	−4.4	10.0	−30.7	−168.8	−4.0	11.4	11.5	13.2
gt–gt–gg–gt-c	−7.7	−26.1	−28.0	−171.0	−9.4	−24.1	6.9	7.6
gt–gt–gg–gt-r	3.7	19.1	−27.8	−164.4	−3.0	10.1	12.6	14.1
gt–gg–gt–gt-c	−10.3	−17.9	−22.8	−157.5	−9.7	−25.9	7.8	8.5
gt–gg–gt–gt-r	−4.6	10.0	−30.9	−171.5	2.1	13.4	11.3	11.3
tg Type								
gt–gt–tg–gg-c	−8.0	−26.6	−35.3	−176.0	−8.1	−12.4	6.5	11.2
gt–gt–tg–gg-r	6.0	17.4	−29.3	−158.7	6.6	12.7	9.3	13.7
gg–gt–tg–tg-r	−5.9	11.7	−30.1	−157.0	−4.0	9.6	9.1	14.6
tg–gt–tg–gt-c	−8.0	−25.2	−24.7	−169.7	−9.5	−23.8	7.0	8.9
tg–gg–tg–gt-c	−7.4	−22.0	−29.3	−152.4	−10.2	−23.4	6.5	10.6
gg–gt–tg–gg-c	−8.3	−24.5	−34.9	−175.9	−8.4	−11.3	5.2	9.6
gg–gt–tg–gg-c	−8.3	−24.6	−34.9	−176.0	−8.3	−11.4	5.2	9.6
gt–gt–tg–gg-r	5.8	18.3	−24.5	−160.9	4.8	12.8	12.2	13.6

[a] The dihedral angles are defined as follows: $\phi_{H1}{}^{ab}$ is H1[a]–C1[a]–O1[a]–C4[b], whereas the superscripts label the ring starting from the non-reducing ring labeled as 'a'. $\psi_{H4}{}^{ab}$ is H4[b]–C4[b]–O1[a]–C1[a]. The other ϕ_H/ψ_H dihedrals are defined analog just changing the ring labels.
[b] Electronic energy of the lowest energy syn tg–gg–gt–gg-c conformer is −1581480.2 kcal/mol.
[c] Conformations labeled with a ∼–c′ indicate that the O1[d]–H hydroxyl group is pointing away from the hydrogen bonding network toward the O5[d] ring oxygen.
[d] Conformations labeled with a ∼–r′ indicate that the O2–H hydrogen is rotated away from O1 but maintains the hydrogen bond with the O3–H hydroxyl group. This can occur on the reducing or first non-reducing ring or both.

from those found for the molecules with single stressed positions in Tables 1 and 2. This result suggests that one must energetically stress the molecule significantly in order to allow this combination of conformations.

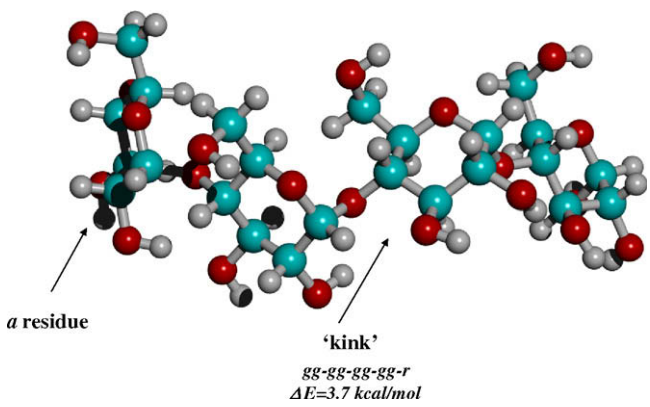

Figure 2. B3LYP/6-311++G** geometry optimized 'r' type DP-4 amylose fragment showing a 'kink' in the center of the molecule.

3.4. Comparison with experimental results

X-ray studies[2,3] of CD26 (Table 4 as well as Table 3 of Ref. 22) clearly show 'band-flip' conformations at two sites that are symmetric to each other. Other cyclic structures[4,5] denoted CA-10 and CA-14 (see Table 3 of Ref. 22) also have 'band-flip' conformations. The experimental dihedral angle values of all the 'band-flip' sites documented, as defined by ϕ_C(O5–C1–O1–C4′) and ψ_C(C1–O1–C4′–C3′), are in very good agreement ϕ_C(+82° to +89°) and ψ_C(−48° to −69°) with the calculated ϕ_H/ψ_H values listed in Table 1 when defined similarly to the experimental values (i.e., ϕ_C(+85° to +90°) and ψ_C(−44° to −57°).

'Kink' conformations have also been found next in sequence to the 'band-flips' in the CA-10 and CA-14 cyclodextrin structures and have values as defined above of ϕ_C(+76° to +93°) and ψ_C(+84° to +92°). These experimental values are again in very good agreement with our 'kink' values, found to be ϕ_C(+60° to +74°) and ψ_C(+72° to +84°), respectively, for the lower energy forms.

It is of interest to discuss the conformations taken up by maltotetraose when bound to enzymes.[7,29,30] For example, the X-ray crystal structure of four product-complexed single mutants of maltotetraose forming amylase[29] with DP-4 bound in the active

Table 2
B3LYP/6-311++G** relative energies, conformations (ϕ_H/ψ_H dihedral angles in °), and dipole moments of 'kink' type DP-4 amylose fragments

Conformer	Dihedral angles[a]						ΔE (kcal/mol)	Dipole (Debye)
	$\phi_{H1}{}^{ab}$	$\psi_{H4}{}^{ab}$	$\phi_{H1}{}^{bc}$	$\psi_{H4}{}^{bc}$	$\phi_{H1}{}^{cd}$	$\psi_{H4}{}^{cd}$		
All gg, gt, and tg								
gg–gg–gg–gg-c	−8.3	−19.3	−57.4	−51.8	−8.7	−21.7	7.4	3.2
gg–gg–gg–gg-r	−0.4	15.8	−48.2	−38.9	4.5	15.9	3.7	13.3
gt–gt–gt–gt-c	−8.6	−25.4	−52.0	−98.1	−9.7	−24.1	11.6	8.8
gt–gt–gt–gt-c″[b]	−7.6	−25.5	−48.3	−51.0	−9.1	−24.3	11.8	5.4
gt–gt–gt–gt-r	−4.4	10.1	−45.1	−41.6	1.2	13.5	7.4	10.1
gt–gt–gt–gt-r″[c]	−10.3	−26.9	−43.6	−40.2	2.8	14.4	7.6	11.4
tg–tg–tg–tg-c	Not observed							
tg–tg–tg–tg-r	0.2	16.9	−43.7	−41.2	1.1	16.0	9.7	8.6
Mixed Forms								
gg–gt–gg–tg-r	−3.3	10.9	76.4	30.4	−6.0	−35.3	17.4	12.7
gg–gt–gg–gg-r	−6.5	14.2	−56.0	−45.6	4.4	16.4	5.7	12.7
Kink in the 1st bridge								
gt–gt–gg–gg-r	−43.3	−39.7	0.9	10.8	4.3	16.5	4.0	10.6
gt–gt–gg–gt-r	−43.4	−39.6	−1.2	9.1	−3.0	13.8	5.1	10.8
gt–gt–gt–gg-r	−43.3	−40.2	5.8	14.5	−3.0	9.7	5.4	9.3
gt–gt–gt–gt-r	−44.0	−40.5	7.3	15.2	4.0	15.9	7.2	10.1
tg–gt–gt–gt-r	−41.8	−38.7	5.6	14.9	2.7	14.9	7.5	10.3

[a] See footnotes in Table 1.
[b] Conformations labeled with a ∼−c″ indicate that the O3[c]−H hydroxyl group is pointing up from the hydrogen bonding network.
[c] In this case the C1[a]–C2[a]–O2[a]–H has a dihedral angle of ∼(+20°) instead of the typical dihedral of ∼(−40°).

site showed 'kink' conformations in the carbohydrate substrate (see Table 4). The average $\phi_{C'}$ and $\psi_{C'}$ values from four crystal structures (see Table 4 for definitions) are 77.4° and −147.9°, respectively, in reasonable agreement with our calculated values, which are not under stress from external sources, as are the enzyme-bound substrates. Other protein crystal structures[7,30] of maltotetraose bound to MBP (maltodextrin-binding protein) and soybean β-amylose, respectively, also show good agreement with the calculated values (Table 4).

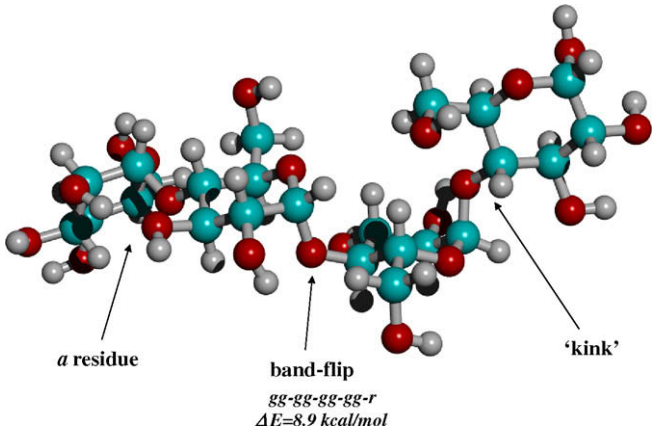

Figure 3. B3LYP/6-311++G** geometry optimized 'r' type DP-4 amylose fragment showing a band-flip followed by a kink.

Internal coordinates, that is, dihedral angles for the three different motifs, are presented in Tables 5–7. Examination of the hydroxymethyl groups on the *b* and *c* residues in Table 5 shows the greatest deviations from the standard gauche/*trans* values of 60°/180°, with the CCOH dihedral angles having a spread of nearly 60° on the *b* residue for the all-gt conformers. The OCCO dihedral angles in the all-gt forms also show some spread, ∼30°, for this residue. Considerable variation in these dihedral angles occurs also in the all-tg series. Residue *c* showed very small deviations in the hydroxymethyl rotamers in the all-gg and all-gt conformers, with some deviations in the all-tg forms.

In Table 6, the values of the dihedral angles for the 'kink' conformations are shown, and we see that there is very little stress being put on the hydroxyl CCOH or the OCCO dihedral groups as a result of the formation of stable 'kink' structures.

The combination 'band-flip/kink' rotamers again showed some significant deviations from the gauche/*trans* normal conformations, in particular, those at the CCOH of ring *b*.

Table 3
B3LYP/6-311++G** relative energies, conformations (ϕ_H/ψ_H dihedral angles in °), and dipole moments of 'band-flip/kink' combinations within DP-4 amylose fragments

Conformer	Dihedral angles[a]						ΔE (kcal/mol)	Dipole (Debye)	Type[b]
	$\phi_{H1}{}^{ab}$	$\psi_{H4}{}^{ab}$	$\phi_{H1}{}^{bc}$	$\psi_{H4}{}^{bc}$	$\phi_{H1}{}^{cd}$	$\psi_{H4}{}^{cd}$			
All gg and gt									
gg–gg–gg–gg-r	−48.5	−37.8	−40.3	−179.2	5.4	15.3	9.0	12.6	k–bf–s
gg–gg–gg–gg-r	1.1	17.1	−42.1	174.0	−55.7	−41.6	8.9	12.8	s–bf–k
gt–gt–gt–gt-r	−48.3	−37.9	−41.2	175.0	−55.7	−41.6	10.2	11.9	k–bf–k
Mixed Forms									
gt–gt–gg–gg-r	−46.6	−40.5	−31.5	−160.2	3.2	10.9	15.0	10.3	k–bf–s
gt–gt–gg–gt-r	−6.3	9.0	−52.8	162.9	−41.9	−40.1	11.8	6.5	s–bf–k
gt–gt–gt–gg-r	−46.2	−39.9	−30.8	−161.5	−42.4	−38.6	16.6	10.8	k–bf–k
gg–gt–gg–tg-r	−41.8	−37.0	−23.8	−160.5	7.0	14.3	9.2	11.0	k–bf–n
gg–gt–gg–gg-r	−45.5	−39.5	−26.3	−164.4	−3.5	10.2	12.9	11.8	k–bf–n

[a] See footnotes in Table 1.
[b] Type: k stands for kink; bf stands for band flip; and s stands for syn form.

Table 4
Calculated and experimental dihedral angles, glycosidic angles, and virtual angles from the X-ray structure of cycloamylose, CA26,[a,b] and maltotetraose[c,d,e]

Dihedral angles	X-ray[a]		X-ray[b]		Syn		Calculated values[f]		Syn	
	ϕ	ψ	ϕ	ψ	ϕ^{ab}	ψ^{ab}	ϕ^{bc}	ψ^{bc}	ϕ^{cd}	ψ^{cd}
Max(bf)	90.2	−51.7	89.6	−51.0			'c' 94.3	−30.8		
							'r' 94.2	−43.2		
Min(bf)	86.4	−45.8	87.8	−47.6			'c' 86.6	−56.2		
							'r' 63.9	−85.3		
Mean(bf)							'c' 90.9	−42.6		
							'r' 82.5	−55.8		
	88.1	−48.4	88.7	−49.3			86.9	−48.9		

(ϕ = O5–C1–O1–C4′) and (ψ = C1–O1–C4′–C3′)

Maltotetraose

	Quiocho[d]		Mikami[e]		Hasegawa[c]			Calculated[g]	
	ϕ	ψ	ϕ	ψ	ϕ	ψ		ϕ	ψ
Glc3–4	86.9	−160.5	76.9	−147.3	78.4	−148.9	'c'	64.7	Kink −168.5
(ϕ_C = ϕ = O5–C1–O4′–C4′), ($\psi_{C'}$ = ψ = C1–O4′–C4′–C5′)							'r'	72.2	Kink −159.0

Glycosidic bond angle C1–O1–C4 (°)			Calculated at central bonds all syn-gg/gt		Calculated[h] at central bonds bf	
	X-ray[a]	X-ray[b]	'c'	'r'	'c'	'r'
Max	120.7	121.6	119.6	119.7	121.2	122.2
Min	114.6	114.6	117.6	117.0	118.8	118.8
Mean	118.3	118.0	118.1	118.9	120.0	119.9

Virtual angle O4–O4′–O4″ (°)	X-ray[a] Helical	X-ray[b] bf	Calculated for syn-gg/gt		Calculated[h] bf	
			'c'	'r'	'c'	'r'
Max	136.7	149.8	136.2	142.1	158.8	147.5
Min	117.9	138.7	130.1	128.5	141.8	131.5
Mean	126.4	143.6	134.6	133.0	151.2	141.4

[a] See Ref. 2.
[b] See Ref. 3.
[c] See Ref. 7.
[d] See Ref. 29.
[e] See Ref. 30.
[f] Values calculated from gg and gt conformations listed in Table 1.
[g] Values calculated from conformations listed in Table 2.
[h] Values calculated from gg and gt conformations listed in Table 8.

In Tables 8–10, we list several structural parameters, that is, chain lengths ($O4^a$–$O4^d$), glycosidic bond angles, and virtual angles that define the molecular dimensions. The $O4^a$–$O4^d$ distances for the 'band-flip' structures are in the range of 11.3–12.6 Å, while the distances are shorter in the 'kink' structures, and somewhat in between for the mixed forms. The C–O–C bond angle at the glycosidic bonds shows significant enlargement at the *bc* 'band-flip' linkage relative to the two end glycosidic bonds, but this enlargement is not found at the 'kink' structures. Also, the virtual angle, $O4^b$–$O4^c$–$O4^d$, is much larger for the 'band-flip' than the *abc* virtual angle. This difference is also found in Table 9 for the 'kink' structures, but not so significantly in the combination forms of Table 10.

3.5. COSMO optimization results

In Tables 11 and 12, results obtained from selecting several previously optimized conformations and re-optimizing at the large basis set, but now including the solvation simulation method, COSMO, are shown.[28] The all-gg-r 'kink' conformation remains lower in energy than the 'c' form by approximately the same amount as the in vacuo case, given in Table 2. However, the relative energy of the all-gt-r 'kink' listed in Table 11 has dropped to ΔE ~3.1 kcal/mol from a value of ~7.7 kcal/mol, a change of over 4 kcal/mol, and this is a significant relative energy lowering as a result of the implicit solvation method, COSMO.[28] Interestingly, the ϕ_H/ψ_H dihedral angles for the 'r' forms do not change significantly, although the 'c' forms do show some small differences.

In the case of 'band-flip' conformers, the all-gg-r (COSMO) relative energy is now smaller than that of the 'c' COSMO form, and this is a reversal of the in vacuo forms, where 'c' was of lower energy. The all-gt-r (COSMO) 'band-flip' relative energy remains higher than that of the comparable 'c' form, which is consistent with the in vacuo results in Table 1. The equivalent sets of dihedral angles are similar for the COSMO versus in vacuo results. It remains true that the all-tg-r/c (COSMO) results remain at much higher energies, in both the 'c' and 'r' forms.

Table 12 lists the important dihedral angles, chain length parameters, glycosidic bond angles, and virtual angles. The results in Table 12 are very comparable to those found in Table 6 for the 'kink' and Table 5 for 'band-flip' conformations.

4. Summary

The work reported here has considerable significance in the overall understanding of carbohydrate structural motifs that determine conformation and their energy relation ships. It should be noted that X-ray structures do not provide relative energies, thus this work fills an important information void. Our results are in agreement with the previous description of these motifs,[2–5] that is, we do not find that a 'kink' conformation is necessary near the 'band-flip', when the molecule is not in a stressed or strain-induced condition. In fact, it was found that 'band-flip/kink' combinations are of higher energy than the single motifs structures. In summary, the patterns developed from this and previous work now include

Table 5
B3LYP/6-311++G** conformations of 'band-flip' type DP-4 amylose fragments, dihedral angles (°) for the hydroxymethyl groups

Conformer	Ring a		Ring b		Ring c		Ring d	
	OCCO[a]	CCOH[b]	OCCO	CCOH	OCCO	CCOH	OCCO	CCOH
All gg, gt, and tg								
gg–gg–gg–gg-c	−64.5	63.4	−59.8	58.4	−59.1	62.0	−58.1	58.8
gg–gg–gg–gg-c'	−64.4	63.5	−59.9	58.7	−59.1	61.6	−58.3	57.0
gg–gg–gg–gg-r	−57.4	56.1	−60.6	59.2	−63.4	61.5	−62.7	63.2
gt–gt–gt–gt-c	60.3	−56.5	54.4	−81.8	59.3	−55.8	62.5	−52.1
gt–gt–gt–gt-r	58.9	−64.0	48.7	−50.0	64.7	−57.1	60.9	−57.5
gt–gt–gt–gt-r'	65.4	−58.0	71.6	−25.7	63.6	−60.7	60.9	−58.0
tg–tg–tg–tg-c	−175.9	−174.6	167.7	69.8	146.2	55.9	165.1	72.4
tg–tg–tg–tg-c'	−175.8	−174.6	168.1	69.9	146.0	55.7	163.4	71.1
tg–tg–tg–tg-r	167.1	50.4	158.2	73.3	−178.9	71.6	159.4	75.8
Mixed gg and gt								
gg–gt–gg–gg-c	−64.5	61.8	69.4	−165.3	−59.2	60.6	−58.0	58.4
gg–gt–gg–gg-r	−58.1	58.3	73.4	−28.9	−59.9	59.9	−62.7	63.5
gg–gg–gt–gg-c	−64.4	63.5	−60.0	58.7	61.3	−57.1	−61.8	62.1
gg–gg–gt–gg-r	−57.4	56.2	−60.8	59.5	56.7	−60.7	−63.5	64.5
gg–gt–gt–gg-c	−64.7	62.7	54.1	−80.0	61.2	−57.4	−60.9	61.2
gg–gt–gt–gg-r	−58.1	57.5	60.1	−75.1	65.3	−56.1	−67.0	68.5
gt–gg–gg–gt-c	63.1	−57.0	−63.9	62.3	−59.2	61.2	62.1	−51.5
gt–gg–gg–gt-r	58.6	−60.0	−61.0	61.5	−59.3	60.0	63.4	−60.4
gt–gt–gg–gt-c	60.2	−56.2	54.1	−81.3	−59.4	60.7	62.7	−51.9
gt–gt–gg–gt-r	65.5	−57.5	70.9	−23.7	−60.0	61.1	63.5	−60.6
gt–gg–gt–gt-c	63.3	−57.2	−64.1	62.5	59.2	−55.8	62.0	−51.9
gt–gg–gt–gt-r	58.7	−60.6	−61.1	61.4	66.1	−64.0	61.5	−59.3
tg Type								
gt–gt–tg–gg-c	60.4	−56.9	55.5	−79.6	142.8	79.5	−58.0	58.8
gt–gt–tg–gg-r	64.9	−57.1	70.0	−27.4	158.7	179.7	−62.3	62.9
gg–gt–tg–tg-r	−57.9	57.6	71.3	−31.9	143.7	−78.6	163.5	76.2
tg–gt–tg–gt-c	−178.0	178.7	54.3	−78.9	−168.1	−44.7	62.9	−52.3
tg–gg–tg–gt-c	−178.3	178.9	−60.5	59.6	141.2	60.0	61.7	−51.8
gg–gt–tg–gg-c	−64.8	63.0	54.9	−77.9	142.7	79.6	−58.0	58.9
gg–gt–tg–gg-c	−64.8	62.9	54.9	−77.7	142.7	79.5	−58.0	58.8
gt–gt–tg–gg-r	65.0	−57.9	70.1	−31.6	179.3	71.8	−62.0	62.8

[a] OCCO is defined as O5–C5–C6–O6 at the specified ring.
[b] CCOH is defined as C5–C6–O6–H at the specified ring.

Table 6
B3LYP/6-311++G** conformations of 'kink' type DP-4 amylose fragments, dihedral angles (°) for the hydroxymethyl groups

Conformer	Ring a		Ring b		Ring c		Ring d	
	OCCO[a]	CCOH	OCCO	CCOH	OCCO	CCOH	OCCO	CCOH
All gg, gt, and tg								
gg–gg–gg–gg-c	−64.3	63.1	−58.8	56.6	−63.7	64.6	−58.7	59.1
gg–gg–gg–gg-r	−57.6	56.8	−61.3	61.6	−64.1	61.5	−62.7	63.3
gt–gt–gt–gt-c	60.3	−56.9	72.3	−66.0	59.7	−55.3	61.4	−51.2
gt–gt–gt–gt-c″	60.5	−55.8	58.9	−58.5	59.9	−56.2	61.4	−51.1
gt–gt–gt–gt-r	60.8	−61.9	57.8	−58.0	61.4	−64.9	60.4	−58.8
gt–gt–gt–gt-r″	60.4	−56.4	59.5	−59.7	61.2	−63.6	60.6	−58.9
tg–tg–tg–tg-r	167.1	50.1	155.8	74.4	160.2	50.1	157.4	75.6
Mixed forms								
gg–gt–gg–tg-c	−57.9	56.8	68.3	62.4	−70.6	65.1	160.8	48.3
gg–gt–gg–gg-r	−58.1	57.9	58.7	−55.4	−66.6	61.9	−62.8	63.5
tg Type								
gt–gt–gg–gg-r	59.6	−58.1	57.9	−62.3	−62.6	62.5	−62.8	63.4
gt–gt–gg–gt-r	59.6	−58.1	57.7	−62.9	−63.3	64.3	62.5	−59.6
gt–gt–gt–gg-r	59.6	−58.2	61.4	−61.4	58.6	−62.4	−63.5	64.9
gt–gt–gt–gt-r	59.6	−58.2	62.1	−61.1	62.8	−61.2	60.9	−58.5
tg–gt–gt–gt-r	165.4	51.3	62.2	−61.0	62.6	−61.6	60.8	−58.6

[a] See footnotes in Table 5.

Table 7
B3LYP/6-311++G** conformations of 'band-flip/kink' combinations[a] within DP-4 amylose fragments, dihedral angles (°) for the hydroxymethyl groups

Conformer	Ring a		Ring b		Ring c		Ring d	
	OCCO[b]	CCOH	OCCO	CCOH	OCCO	CCOH	OCCO	CCOH
All gg and gt								
gg–gg–gg–gg-r	−57.5	57.1	−62.0	58.8	−63.2	61.4	−62.7	63.2
gg–gg–gg–gg-r	−57.2	55.8	−60.4	57.1	−62.7	61.8	−65.7	63.1
gt–gt–gt–gt-r	−57.3	56.9	−61.8	56.7	−62.6	61.7	−65.8	63.4
Mixed forms								
gt–gt–gg–gg-r	59.5	−57.7	71.7	−29.8	63.7	−60.5	60.9	−57.9
gt–gt–gg–gt-r	60.4	−61.8	55.5	−67.0	60.4	−58.9	61.4	−59.1
gt–gt–gt–gg-r	59.7	−58.0	71.4	−30.4	59.5	−58.2	60.5	−59.0
gg–gt–gg–tg-r	59.3	−56.5	69.4	−32.2	−179.4	67.6	−62.6	63.0
gg–gt–gg–gg-r	59.1	−56.7	70.6	−27.4	−60.1	61.1	63.5	−60.4

[a] See footnotes in Table 3.
[b] See footnotes in Table 5.

Table 8
B3LYP/6-311++G** conformations of 'band-flip' type DP-4 amylose fragments, chain length, glycosidic bond angle, and virtual angles

Conformer	$O4^a$–$O4^d$ (Å)	$O1^a$–$O1^d$ (Å)	$C1^a$–$O1^a$–$C4^b$ (°)	$C1^b$–$O1^b$–$C4^c$ (°)	$C1^c$–$O1^c$–$C4^d$ (°)	$O4^a$–$O4^b$–$O4^c$ (°)	$O4^b$–$O4^c$–$O4^d$ (°)
All gg, gt, and tg							
gg–gg–gg–gg-c	12.59	12.05	118.4	120.1	118.2	133.5	156.1
gg–gg–gg–gg-c'	12.57	11.83	118.3	120.1	118.5	133.5	156.3
gg–gg–gg–gg-r	12.11	11.47	118.8	120.8	118.7	133.0	132.5
gt–gt–gt–gt-c	12.24	11.54	117.7	119.4	117.9	136.5	141.8
gt–gt–gt–gt-r	10.39	9.76	119.4	122.2	118.3	132.7	108.7
gt–gt–gt–gt-r'	12.61	11.17	119.3	118.8	119.5	133.8	142.4
tg–tg–tg–tg-c	12.48	12.39	119.6	121.2	119.6	129.6	158.8
tg–tg–tg–tg-c'	12.48	12.13	119.6	121.1	119.7	129.8	158.2
tg–tg–tg–tg-r	12.57	11.30	119.5	119.0	119.7	133.3	147.1
Mixed gg and gt							
gg–gt–gg–gg-c	12.39	11.45	118.2	118.8	118.3	135.2	146.0
gg–gt–gg–gg-r	12.47	11.41	119.5	118.9	118.7	131.7	141.2
gg–gg–gt–gg-c	12.60	12.24	118.5	120.0	118.0	132.8	156.8
gg–gg–gt–gg-r	12.03	11.31	118.9	120.4	119.2	132.5	131.5
gg–gt–gt–gg-c	12.30	11.53	117.8	119.4	118.2	136.7	142.9
gg–gt–gt–gg-r	12.10	11.99	119.5	120.5	116.3	131.2	134.2
gt–gg–gg–gt-c	12.71	12.26	117.7	120.1	117.7	135.8	155.5
gt–gg–gg–gt-r	12.14	11.47	119.3	119.9	119.5	129.5	144.7
gt–gt–gg–gt-c	12.23	11.49	117.8	119.4	117.8	135.8	143.3
gt–gt–gg–gt-r	12.57	11.51	119.2	119.2	119.6	132.4	147.5
gt–gg–gt–gt-c	12.74	12.31	117.6	119.8	117.7	136.3	154.6
gt–gg–gt–gt-r	12.13	11.53	119.3	119.7	119.4	129.6	142.9
tg Type							
gt–gt–tg–gg-c	12.08	11.48	117.8	120.5	118.7	136.3	138.7
gt–gt–tg–gg-r	12.64	11.52	119.2	119.4	118.9	133.8	147.7
gg–gt–tg–tg–r	12.43	11.67	119.5	119.7	120.0	129.7	150.4
tg–gt–tg–gt-c	12.20	11.18	117.7	119.5	117.9	135.9	142.5
tg–gg–tg–gt-c	12.57	12.43	118.0	120.8	117.8	134.4	155.4
gg–gt–tg–gg-c	12.14	11.49	117.8	120.5	118.7	137.2	138.8
gg–gt–tg–gg-c	12.14	11.48	117.8	120.5	118.7	137.2	138.7
gt–gt–tg–gg-r	12.68	11.24	119.1	118.5	119.0	134.1	147.4

multiple syn type conformations, as well as energy stressed 'kink' and 'band-flip' forms. Moreover, our investigations indicate that hydroxyl directions (i.e., 'c' and 'r') and hydroxymethyl conformations (gg, gt, and tg) direct the energetic stability of the molecules preparing one form or the other to best fit the requirements of the particular macromolecular system, such as double helices, V-helices, and chain-reversals . DP-4 conformers have enhanced our previous conclusions, that is, confirming that the disaccharide maltose is a poor choice for modeling larger macromolecular molecules. Maltose remains a model for establishing specific end effects, showing how the tg conformation may appear favorable at the non-reducing end.

Overall, the density functional method has proven to be remarkably useful in the investigation of structure and energy relationships of carbohydrates. Structural information obtained from DFT calculations is consistent with the few high-resolution X-ray structures available, and it is this consistency that allows us to use this computational tool as a predictive solution to numerous carbohydrate problems.

To date, we have not answered the question of how the energy-stressed conformers studied here are experimentally formed, and work on the energy barrier for accessing these states remains to be determined.

Table 9
B3LYP/6-311++G** conformations of 'kink' type DP-4 amylose fragments, chain length, glycosidic bond angle, and virtual angles

Conformer	$O4^a$–$O4^d$ (Å)	$O1^a$–$O1^d$ (Å)	$C1^a$–$O1^a$–$C4^b$ (°)	$C1^b$–$O1^b$–$C4^c$ (°)	$C1^c$–$O1^c$–$C4^d$ (°)	$O4^a$–$O4^b$–$O4^c$ (°)	$O4^b$–$O4^c$–$O4^d$ (°)
All gg, gt, and tg							
gg–gg–gg–gg-c	11.42	12.28	118.1	118.1	118.0	135.2	147.8
gg–gg–gg–gg-r	11.25	11.88	119.1	116.5	118.8	131.2	145.8
gt–gt–gt–gt-c	12.40	12.80	117.9	121.0	117.8	136.2	168.6
gt–gt–gt–gt-c″	11.49	12.17	117.9	118.6	117.9	135.8	148.8
gt–gt–gt–gt-r	11.59	11.98	119.5	117.0	119.4	132.9	149.6
gt–gt–gt–gt-r″	12.12	11.90	117.2	116.8	119.5	143.0	149.0
tg–tg–tg–tg-r	12.01	12.32	119.6	116.0	119.6	135.7	151.5
Mixed forms							
gg–gt–gg–tg-r	10.59	12.24	119.7	122.9	116.4	128.1	134.8
gg–gt–gg–gg-r	11.12	12.12	119.7	117.8	118.7	129.1	145.7
Kink in the 1st bridge							
gt–gt–gg–gg-r	11.79	10.41	116.8	119.3	118.8	149.5	129.4
gt–gt–gg–gt-r	11.78	10.24	116.8	119.3	119.6	149.5	129.2
gt–gt–gt–gg-r	11.76	10.22	116.9	119.5	119.3	149.8	129.3
gt–gt–gt–gt-r	11.88	10.44	116.9	119.4	119.4	149.7	130.8
tg–gt–gt–gt-r	11.86	10.34	116.5	119.5	119.5	150.7	130.1

Table 10
B3LYP/6-311++G** conformations of 'band-flip/kink' combinations[a] within DP-4 amylose fragments, chain length, glycosidic bond angle, and virtual angles

Conformer	$O4^a$–$O4^d$ (Å)	$O1^a$–$O1^d$ (Å)	$C1^a$–$O1^a$–$C4^b$ (°)	$C1^b$–$O1^b$–$C4^c$ (°)	$C1^c$–$O1^c$–$C4^d$ (°)	$O4^a$–$O4^b$–$O4^c$ (°)	$O4^b$–$O4^c$–$O4^d$ (°)
All gg and gt							
gg–gg–gg–gg-r	11.54	11.40	116.6	120.8	118.8	147.2	130.9
gg–gg–gg–gg-r	11.88	11.81	118.8	121.0	117.5	133.3	126.9
gt–gt–gt–gt-r	11.34	11.87	116.6	121.0	117.4	147.3	126.8
Mixed forms							
gt–gt–gg–gg-r	12.27	11.13	117.2	118.7	119.5	149.1	141.1
gt–gt–gg–gt-r	10.76	10.75	119.6	121.7	117.4	132.3	112.3
gt–gt–gt–gg-r	12.40	12.11	117.0	118.9	116.9	148.9	141.3
gg–gt–gg–tg-r	12.55	11.58	117.0	118.7	118.8	148.9	147.4
gg–gt–gg–gg-r	12.44	11.57	117.3	119.2	119.5	148.7	147.1

[a] See footnotes in Table 3.

Table 11
COSMO B3LYP/6-311++G** energies and conformations (ϕ_H/ψ_H dihedral angles in °) of 'kink' and 'band-flip' type DP-4 amylose fragments

Conformer	Dihedral angles[a]						ΔE[b] (kcal/mol)	Dipole (Debye)
	$\phi_{H1}{}^{ab}$	$\psi_{H4}{}^{ab}$	$\phi_{H1}{}^{bc}$	$\psi_{H4}{}^{bc}$	$\phi_{H1}{}^{cd}$	$\psi_{H4}{}^{cd}$		
Kink								
All gg								
gg–gg–gg–gg-c	−6.74	−0.7	−47.7	−39.0	−8.9	−8.8	6.5	3.4
gg–gg–gg–gg-r	−3.00	13.0	−48.0	−39.6	−3.3	10.5	2.2	16.0
All gt								
gt–gt–gt–gt-c	−6.94	−12.2	−61.8	−77.4	−10.0	−13.1	9.0	11.5
gt–gt–gt–gt-r	−2.53	11.2	−42.5	−40.2	−2.8	8.0	3.1	11.6
All tg								
tg–tg–tg–tg-c	Not observed							
tg–tg–tg–tg-r	0.30	14.1	−41.4	−42.2	2.0	13.8	8.1	10.5
Band-flip								
All gg								
gg–gg–gg–gg-c	−7.28	−2.3	−23.8	−156.5	−10.2	−9.5	6.4	5.5
gg–gg–gg–gg-r	−2.11	12.8	−36.9	−175.3	−3.4	8.5	5.1	15.7
All gt								
gt–gt–gt–gt-c	−7.70	−11.4	−27.8	−167.9	−9.0	−12.1	4.7	13.1
gt–gt–gt–gt-r	−4.29	9.4	−53.7	157.2	26.9	13.8	8.0	5.1
All tg								
tg–tg–tg–tg-c	−3.12	5.8	−30.2	−147.5	−3.2	8.5	9.8	15.5
tg–tg–tg–tg-r	0.56	14.1	−24.0	−167.2	2.1	12.2	9.1	9.0

[a] See Table 1 for definition of dihedral angles.
[b] Electronic energy of the lowest energy syn conformer gg–gg–gg–gg-r is −1581524.4 kcal/mol.

Table 12
COSMO B3LYP/6-311++G** conformations of 'kink' and 'band-flip' type DP-4 amylose fragments, dihedral angles (°) for the hydroxymethyl groups, chain length, glycosidic bond angle, and virtual angles

Kink								
Conformer	Ring a		Ring b		Ring c		Ring d	
	OCCO[a]	CCOH[2]	OCCO	CCOH	OCCO	CCOH	OCCO	CCOH
All gg								
gg–gg–gg–gg–c	−62.6	61.8	−60.9	60.9	−65.2	63.3	−60.6	61.6
gg–gg–gg–gg-r	−61.4	60.7	−61.9	61.9	−65.0	62.8	−61.8	62.0
All gt								
gt–gt–gt–gt-c	63.4	−62.9	67.2	−76.6	62.2	−61.9	63.8	−58.5
gt–gt–gt–gt-r	63.0	−65.6	63.2	−60.0	60.0	−64.2	63.0	−58.6
All tg								
tg–tg–tg–tg-r	166.7	50.7	156.7	74.0	157.8	46.9	158.2	74.4

	$O4^a$–$O4^d$ (Å)	$O1^a$–$O1^d$ (Å)	$C1^a$–$O1^a$–$C4^b$ (°)	$C1^b$–$O1^b$–$C4^c$ (°)	$C1^c$–$O1^c$–$C4^d$ (°)	$O4^a$–$O4^b$–$O4^c$ (°)	$O4^b$–$O4^c$–$O4^d$ (°)
All gg							
gg–gg–gg–gg-c	10.77	11.75	119.3	117.1	118.5	128.4	142.1
gg–gg–gg–gg-r	11.16	11.76	119.3	117.2	119.1	130.3	145.4
All gt							
gt–gt–gt–gt-c	11.66	12.63	118.9	119.1	118.2	130.5	159.3
gt–gt–gt–gt-r	11.17	11.68	119.6	117.3	119.4	129.6	146.9
All tg							
tg–tg–tg–tg-r	11.73	12.14	119.5	116.4	119.4	133.1	150.5

Band-flip								
Conformer	Ring a		Ring b		Ring c		Ring d	
	OCCO[a]	CCOH[a]	OCCO	CCOH	OCCO	CCOH	OCCO	CCOH
All gg								
gg–gg–gg–gg-c	−62.7	62.1	−61.5	62.0	−61.3	62.1	−60.4	61.6
gg–gg–gg–gg-r	−61.3	60.9	−61.3	61.2	−63.1	62.5	−61.6	61.8
All gt								
gt–gt–gt–gt-c	63.4	−62.1	68.6	−158.8	61.8	−61.0	64.0	−58.8
gt–gt–gt–gt-r	62.3	−65.8	49.4	−58.2	64.3	−60.2	63.5	−58.9
All tg								
tg–tg–tg–tg-r	178.4	169.2	160.7	72.8	143.0	57.3	161.2	72.8
tg–tg–tg–tg-r	166.7	50.6	157.9	73.9	177.6	92.3	158.8	74.3

	$O4^a$–$O4^d$ (Å)	$O1^a$–$O1^d$ (Å)	$C1^a$–$O1^a$–$C4^b$ (°)	$C1^b$–$O1^b$–$C4^c$ (°)	$C1^c$–$O1^c$–$C4^d$ (°)	$O4^a$–$O4^b$–$O4^c$ (°)	$O4^b$–$O4^c$–$O4^d$ (°)
All gg							
gg–gg–gg–gg-c	12.49	12.15	119.1	119.9	118.4	129.5	156.3
gg–gg–gg–gg-r	12.05	11.11	119.1	119.9	119.3	131.0	134.6
All gt							
gt–gt–gt–gt-c	12.33	11.64	118.7	118.4	118.5	131.8	144.9
gt–gt–gt–gt-r	10.41	9.72	119.3	122.0	118.1	131.1	107.9
All tg							
tg–tg–tg–tg-r	12.58	12.52	119.5	121.2	119.3	129.5	160.8
tg–tg–tg–tg-r	12.40	11.16	119.3	119.3	119.4	131.7	145.9

[a] See Table 5 for dihedral angle definitions.

Supplementary data

Supplementary data associated with this article can be found, in the online version, at doi:10.1016/j.carres.2008.11.016.

References

1. Schnupf, U.; Willett, J. L.; Bosma, W. B.; Momany, F. A. *Carbohydr. Res.* **2008**, *343*.
2. Gessler, K.; Uson, I.; Takaha, T.; Krauss, N.; Smith, S. M.; Okada, S.; Sheldrick, G. M.; Saenger, W. *Proc. Natl. Acad. Sci. U.S.A.* **1999**, *96*, 4246–4251.
3. Nimz, O.; Gebler, K.; Uson, I.; Saenger, W. *Carbohydr. Res.* **2001**, *336*, 141–153.
4. Jacob, J.; Gebler, K.; Hoffman, D.; Sanbe, H.; Koizumi, K.; Smith, S. M.; Takaha, T.; Saenger, W. *Angew. Chem., Int. Ed.* **1998**, *37*, 606–608.
5. Jacob, J.; Gebler, K.; Hoffman, D.; Sanbe, H.; Koizumi, K.; Smith, S. M.; Takaha, T.; Saenger, W. *Carbohydr. Res.* **1999**, *322*, 228–246.
6. Yoshioka, Y.; Hasegawa, K.; Matsuura, Y.; Katsube, Y.; Kubota, M. *J. Mol. Biol.* **1997**, *271*, 619–628.
7. Hasegawa, K.; Kubota, M.; Matsuura, Y. *Protein Eng.* **1999**, *12*, 819–824.
8. Kimura, T.; Nakakuki, T. *Starch/Stärke* **2006**, *42*, 151–157.
9. Whitlow, K. J.; Gochman, N.; Forrester, R. L.; Wataji, L. *J. Clin. Chem.* **1979**, *25*, 481–483.
10. Momany, F. A.; Willett, J. L. *J. Comput. Chem.* **2000**, *21*, 1204–1219.
11. Momany, F. A.; Willett, J. L. *Carbohydr. Res.* **2000**, *326*, 210–226.
12. Strati, G. L.; Willett, J. L.; Momany, F. A. *Carbohydr. Res.* **2002**, *337*, 1833–1849.
13. Strati, G. L.; Willett, J. L.; Momany, F. A. *Carbohydr. Res.* **2002**, *337*, 1851–1859.
14. Momany, F. A.; Appell, M.; Strati, G. L.; Willett, J. L. *Carbohydr. Res.* **2004**, *339*, 553–567.
15. Momany, F. A.; Appell, M.; Willett, J. L.; Bosma, W. B. *Carbohydr. Res.* **2005**, *340*, 1638–1655.
16. Appell, M.; Willett, J. L.; Momany, F. A. *Carbohydr. Res.* **2005**, *340*, 459–468.
17. Bosma, W. B.; Appell, M.; Willett, J. L.; Momany, F. A. *J. Mol. Struct.:THEOCHEM* **2006**, *776*, 1–19.
18. Bosma, W. B.; Appell, M.; Willett, J. L.; Momany, F. A. *J. Mol. Struct.:THEOCHEM* **2006**, *776*, 13–24.
19. Appell, M.; Strati, G. L.; Willett, J. L.; Momany, F. A. *Carbohydr. Res.* **2004**, *339*, 537–551.
20. Momany, F. A.; Appell, M.; Willett, J. L.; Schnupf, U.; Bosma, W. B. *Carbohydr. Res.* **2006**, *341*, 525–537.
21. Schnupf, U.; Willett, J. L.; Bosma, W. B.; Momany, F. A. *Carbohydr. Res.* **2007**, *342*, 196–216.

22. Momany, F. A.; Schnupf, U.; Willett, J. L.; Bosma, W. B. *Struct. Chem.* **2007**, *18*, 611–632.
23. Schnupf, U.; Willett, J. L.; Bosma, W. B.; Momany, F. A. *Carbohydr. Res.* **2007**, *342*, 2270–2285.
24. Schnupf, U.; Willett, J. L.; Bosma, W. B.; Momany, F. A. *J. Comput. Chem.* **2008**, *29*, 1103–1112.
25. PQS Ab Initio Program Package, Parallel Quantum Solutions, 2013 Green Acres, SuiteE, Fayetteville, AR 72703, USA.
26. InsightII/Discover, Accelrys Corp., 9685 Scranton Road, San Diego, CA 92121-3752, USA.
27. Hyperchem 7.5, Hypercube, Inc., 115 NW 4th Street, Gainesville, FL 32601, USA.
28. Klamt, A.; Schuurmann, G. *J. Chem. Soc., Perkin Trans. 2* **1993**, *5*, 799–805; Baldridge, K.; Klamt, A. *J. Chem. Phys.* **1997**, *106*, 6622–6633.
29. Quiocho, F. A.; Spurlino, J. C.; Rodseth, L. E. *Structure* **1997**, *5*, 997–1015.
30. Mikami, B.; Degano, M.; Hehre, E. J.; Sacchettini, J. C. *Biochemistry* **1994**, *33*, 7779–7787.